Journal of CO2 Utilization 80 (2024) 102701

Contents lists available at ScienceDirect

Journal of CO2 Utilization

journal homepage: www.elsevier.com/locate/jcou

Photocatalytic reduction of CO_2 over Ti^{3+} self-doped TiO_2-based nanomaterials

Rudolf Ricka [a,b], Agnieszka Wanag [c], Ewelina Kusiak-Nejman [c], Dariusz Moszyński [c], Miroslava Filip Edelmannová [a], Martin Reli [a], Zdeněk Baďura [d,e], Giorgio Zoppellaro [d,e], Radek Zbořil [d,e], Antoni W. Morawski [c], Kamila Kočí [a,f,*]

[a] Institute of Environmental Technology, CEET, VŠB-Technical University of Ostrava, 17. listopadu 2172/15, 708 00 Ostrava-Poruba, Czech Republic
[b] Faculty of Materials Science and Technology, VŠB-Technical University of Ostrava, 17. listopadu 2172/15, 708 00 Ostrava-Poruba, Czech Republic
[c] West Pomeranian University of Technology in Szczecin, Faculty of Chemical Technology and Engineering, Department of Inorganic Technology and Environment Engineering, ul. Pułaskiego 10, 70-322 Szczecin, Poland
[d] Regional Centre of Advanced Technologies and Materials, Czech Advanced Technology and Research Institute (CATRIN), Palacký University, Šlechtitelů 27, 783 71 Olomouc, Czech Republic
[e] Nanotechnology Centre, CEET, VŠB-Technical University of Ostrava, 17. listopadu 2172/15, 708 00 Ostrava-Poruba, Czech Republic
[f] Department of Physics and Materials Engineering, Faculty of Technology, Tomas Bata University in Zlín, Vavrečkova 275, Czech Republic

ARTICLE INFO

Keywords:
TiO_2
Ti^{3+} sites
Oxygen vacancies
$NaBH_4$ reduction
CO_2 reduction
Photocatalysis

ABSTRACT

In this study, we explored the photocatalytic efficacy of Ti^{3+}-doped TiO_2-based photocatalysts for CO_2 reduction. The Ti^{3+} self-doped photocatalysts were synthesized using a straightforward chemical reduction with sodium borohydride ($NaBH_4$). Our investigation aimed to elucidate the intricate interplay between the synthesis process and the quantity of $NaBH_4$ reductant on the physical-chemical and photocatalytic attributes of the defective TiO_2-based photocatalysts. We explored three different commercially available TiO_2 materials labeled P25, (S) TiO_2, and KRONOClean7050, which were reduced (2 g of TiO_2) with 0.75 and 1.5 g of $NaBH_4$. The reduction with 0.75 g of $NaBH_4$ led to a significant decrease of photocatalytic activity in all three cases. It was caused by clogging of the photocatalysts surface by sodium ions which resulted in the surface recombination of charge carriers. Oppositely, the reduction with 1.5 g of $NaBH_4$, led to an increase of the photocatalytic activity with superior performance of KRONOClean7050. The comprehensive characterization of all the samples explained this superior performance of KC7050_RED_1.5 sample. Importantly, it did not contain any amorphous phase and the crystal size was two times higher compared to other 2 samples reduced by 1.5 g of $NaBH_4$. In the addition to higher crystallinity, the formation of a disordered TiO_{2-x} layer, enriched with Ti^{3+} defects and oxygen vacancies, was confirmed. These structural features enhance the light absorption and mitigate undesired recombination of photogenerated charge carriers. These results would trigger farther investigation of defect engineering towards enhancement of the efficiency of metal oxide photocatalysts.

1. Introduction

As a consequence of industrialization and rapid population growth in recent years, global energy consumption has increased significantly [1]. According to data published by the United Nations in 2022, the world population has grown by 5.41 billion in the last 62 years, and this trend is expected to continue in the next decades [2,3]. Experts predict that the consumption of energy resources will continue to increase rapidly along with expected fast growing population. Thus, the complete depletion of fossil fuel reserves is expected in the next 100 years [4,5]. In light of these facts, it is essential to find new efficient approaches to provide sustainable energy sources. The photocatalytic processes are considered as one of the most promising technologies to achieve this goal.

Photocatalytic reduction of CO_2 represents an effective strategy to reduce CO_2 molecules while producing valuable compounds such as methane or methanol [6,7]. Since the realization of the first photocatalytic CO_2 reduction experiment in 1979 by Inoue et al. [8], this reaction has aroused enormous interest in the scientific community [9,10].

* Corresponding author at: Institute of Environmental Technology, CEET, VŠB-Technical University of Ostrava, 17. listopadu 2172/15, 708 00 Ostrava-Poruba, Czech Republic.
E-mail address: kamila.koci@vsb.cz (K. Kočí).

https://doi.org/10.1016/j.jcou.2024.102701
Received 15 October 2023; Received in revised form 17 January 2024; Accepted 4 February 2024
Available online 14 February 2024

Photocatalytic reduction of CO_2 represents a very complex chemical process, which can be significantly influenced by various factors [11]. These factors include the crystal structure of the photocatalysts, the presence of defects (for example, oxygen vacancies), the reducing agent used during a CO_2 reduction process, the electronic structure of the investigated photocatalyst samples, or the presence of impurities as subsequently described in this study [12,13]. Although the effectiveness of this process has been demonstrated, the conversion of CO_2 has remained very low, and therefore. Thus, its industrial application is still quite limited [14,15]. Based on these facts, it is very important to design and synthesize new photoactive materials to improve the photocatalytic CO_2 reduction process.

Titanium dioxide (TiO_2) has been the most widely used photocatalyst since the 1970 s. It is applied mainly for its low cost, high chemical stability, and high availability [16–19]. Although this nanomaterial appears to be ideal for photocatalysis, the high recombination rates of the generated charge carriers restrict the photocatalytic efficiency and applicability of TiO_2 [20]. Additionally, this photocatalyst is unsuitable for solar photocatalytic processes due to its wide band gap ($E_g = 3.2$ eV) [21]. Furthermore, it has been confirmed that TiO_2 can harvest less than 5% of solar light [22]. Based on these facts, it is necessary to enhance the photocatalytic activity of this material.

One of the most effective ways to enhance the photocatalytic performance of TiO_2 is to reduce it towards highly defective so called "black TiO_2". This material can be included among the most studied photocatalysts since its discovery by Chen et al. in 2011 [23–25]. It is a defective material with a narrow band gap (2.4 - 2.8 eV) [26]. According to the literature, defects play a key role in the adsorption and activation of CO_2 molecules as they become primary sites and thus have a notable impact on the final selectivity of the photocatalytic CO_2 reduction products [27]. The Ti^{3+} sites and oxygen vacancies (V_o) in the black TiO_2 structure make this material one of the best candidates for various photocatalytic applications, such as photocatalytic reduction of CO_2 [28], photocatalytic hydrogen production [29,30], or photocatalytic degradation of pollutants [31]. The structural defects are responsible not only for the change in the material colour, but also for the enhanced absorption of incident radiation, manifested by a more efficient separation of photoinduced pairs and an increase in photocatalytic activity [24,32–34]. The Ti^{3+} defects and oxygen vacancies, formed on the surface of the black TiO_2 photocatalyst, play a crucial role, especially in averting undesired charge recombination and thus facilitating a more efficient photocatalytic reaction by the formation of new energy levels and the capture of electrons on the surface of the black TiO_2 photocatalyst [30,35]. Despite many published studies on this material there are still many challenges, which have not yet been explored [36].

In this work, two sets of reduced TiO_2 photocatalysts were synthesized using the $NaBH_4$ reduction method, representing a cheap and effective way to obtain defective TiO_2-based photocatalysts [37]. As a result, we proved the significant effect of the starting crystal structure of the photocatalyst and the principal effect of the mutual concentration of borohydride reductant and TiO_2 photocatalyst, which primarily affects the degree of oxygen vacancies ($Ti^{§+}$ ions) and consequently, the efficiency of photocatalytic reduction of CO_2.

2. Experimental section

2.1. Materials

Aeroxide® TiO_2 P25 (Evonik Industries AG, Germany), ((S)TiO_2, Grupa Azoty Zakłady Chemiczne "Police" S.A., Poland) and TiO_2 – KRONOClean 7050 (KC7050, KRONOS International, Inc., USA) were used as various types of TiO_2 photocatalysts. (S)TiO_2 was pre-treated to remove the residual sulphur from post-production sulphur acid. This procedure was described in detail in a previously published article [38]. Sodium borohydride ($NaBH_4$) was purchased from Merck KGaA (Germany), ethanol (C_2H_5OH) from P. P. H. "STANLAB" Sp. z o.o., Poland and methanol (CH_3OH) from PENTA s.r.o.

2.2. Synthesis of defective TiO_2 photocatalysts

Defective, Ti^{3+} self-doped TiO_2 photocatalysts were synthesized by $NaBH_4$ reduction treatment. First, the mixtures of 2.0 g of TiO_2 materials (P25, (S)TiO_2, and KC7050) with 0.75 and 1.5 g of $NaBH_4$ reductant were ground for 30 min in an agate mortar. Subsequently, the powder mixtures of these substances were transferred to a quartz crucible and placed in a tubular furnace, where they were first subjected to 35-minute heating up to 350 °C (temperature rate: 10 °C/min) and then calcined at this temperature for 1 h. This step was carried out in an argon atmosphere (purity 5.0, Messer Polska Sp. z o.o., Poland) with the flow rate of 10 ml/min before calcination started. After calcination, the photocatalysts were left in a tubular furnace and cooled to room temperature under an argon atmosphere. Finally, the cooled samples were removed from the furnace, washed with ethanol followed by washing with water, and dried in an oven at 90 °C overnight. For clarity purposes, the list of all photocatalyst samples investigated in this study is given in Table 1.

2.3. Photocatalytic CO_2 reduction experiments

The photocatalytic reduction of CO_2 was carried out in a batch photoreactor (stainless steel, volume 357 ml, Fig. S1). Individual steps of the photocatalytic experiments are described in the Supplementary Material.

2.4. Characterization of the synthesized photocatalysts

The samples were comprehensively characterized by X-ray diffraction analysis (XRD), Raman spectroscopy, electron paramagnetic resonance (EPR), X-ray photoelectron spectroscopy (XPS), N_2 adsorption-desorption measurements, UV-Vis diffuse reflectance spectroscopy (UV-Vis/DRS), and scanning electron microscopy with energy dispersive spectroscopy (SEM-EDX). A detailed description of the characterization techniques is given in Supplementary Materials.

3. Results and discussion

3.1. Characterization of the photocatalysts

Reference and synthesized TiO_2 photocatalysts were comprehensively characterized using different analytical techniques, and then the correlations between their physical-chemical properties and the photocatalytic activity for a CO_2 reduction were discussed.

X-ray diffraction analysis was performed to define the phase and crystallographic composition of the investigated nanomaterials. Based on the data in Table 2, obtained from the XRD analysis, it was revealed that all TiO_2 samples exhibit the presence of the anatase phase. The presence of this phase corresponds to the black-marked diffraction peaks

Table 1
List of the investigated photocatalyst samples.

Sample designation	Precursor	Amount of $NaBH_4$ used for chemical reduction (g)
P25	P25	0
P25_RED_0.75		0.75
P25_RED_1.5		1.5
(S)TiO_2	(S)TiO_2	0
(S)TiO_2_RED_0.75		0.75
(S)TiO_2_RED_1.5		1.5
KC7050	KC7050	0
KC7050_RED_0.75		0.75
KC7050_RED_1.5		1.5

* All samples were prepared using 2.0 g of TiO_2-based materials (P25, (S)TiO_2, KC7050).

Table 2
Phase composition of the tested TiO_2 photocatalysts.

Sample name	Phase composition			
	Anatase (wt%)	Rutile (wt%)	$Ti_{4.5}O_5$ (wt%)	Amorphous phase (wt%)
P25	91	9	-	-
P25_RED_0.75	25	8	67	-
P25_RED_1.5	11	-	20	69
(S)TiO_2	95	5	-	-
((S)TiO_2 RED_0.75	41	12	-	47
(S)TiO_2 RED_1.5	3	-	-	97
KC7050	29	-	-	71
KC7050_RED_0.75	100	-	-	-
KC7050_RED_1.5	100	-	-	-

shown in Fig. 1 (PDF-2 Card No. 00–021-1272). Furthermore, the XRD patterns of the precursors P25 and (S)TiO_2 with their samples in reduced form (P25_RED_0.75, (S)TiO_2 RED_0.75) demonstrated the coexistence of the rutile phase, as can be observed from the red-marked diffraction peaks (PDF-2 Card No. 01–087-0710). Quantitative analysis confirmed a minority content of this phase in the structure of these four photocatalyst samples (Table 2).

Upon closer examination of the XRD patterns of the P25-based nanomaterials, new diffraction peaks were found in the XRD spectra of the reduced samples P25_RED_0.75 and P25_RED_1.5. These new white-marked diffraction peaks identify the $Ti_{4.5}O_5$ crystallite phase $Ti_{4.5}O_5$ (PDF-2 Card No. 01–071-6414). The mechanism of the formation of this stable phase is not entirely unambiguous. There are different views on the formation of this stable phase. One of them points to the difference in the surface enthalpies of anatase and rutile in commercial P25 and the subsequent transformation of these phases into a disordered TiO_{2-x} layer. The surface enthalpy of the rutile phase is higher than that of anatase, and therefore, reduction from the original rutile to the final disordered TiO_{2-x} layer is facilitated [39]. In contrast, Rempel et al. explained that the formation of this phase is related to the lack of oxygen during the calcination process. Due to the lack of oxygen, complete oxidation to TiO_2 does not occur and therefore intermediate phases are formed, among which the $Ti_{4.5}O_5$ phase can be included [40]. Based on the mentioned facts, it is clear that the formation of this phase has not been adequately investigated. Therefore, it is necessary to continue the detailed analysis of this phase to elucidate its formation mechanism and its influence on the photocatalytic properties of TiO_2-based photocatalysts.

In addition to anatase, rutile, and $Ti_{4.5}O_5$, an amorphous phase was detected in the structures of commercial KC7050 and reduced samples based on P25 (P25_RED_1.5) and (S)TiO_2 ((S)TiO_2 _RED_0.75, (S)TiO_2_RED_1.5). This phase corresponds to broad peaks in the 2θ range between 7 and 15° (Fig. 1). Rietveld analysis of these samples subsequently confirmed the majority of this phase in the contents of these tested photocatalysts. The origin of this phase is related to the synthesis

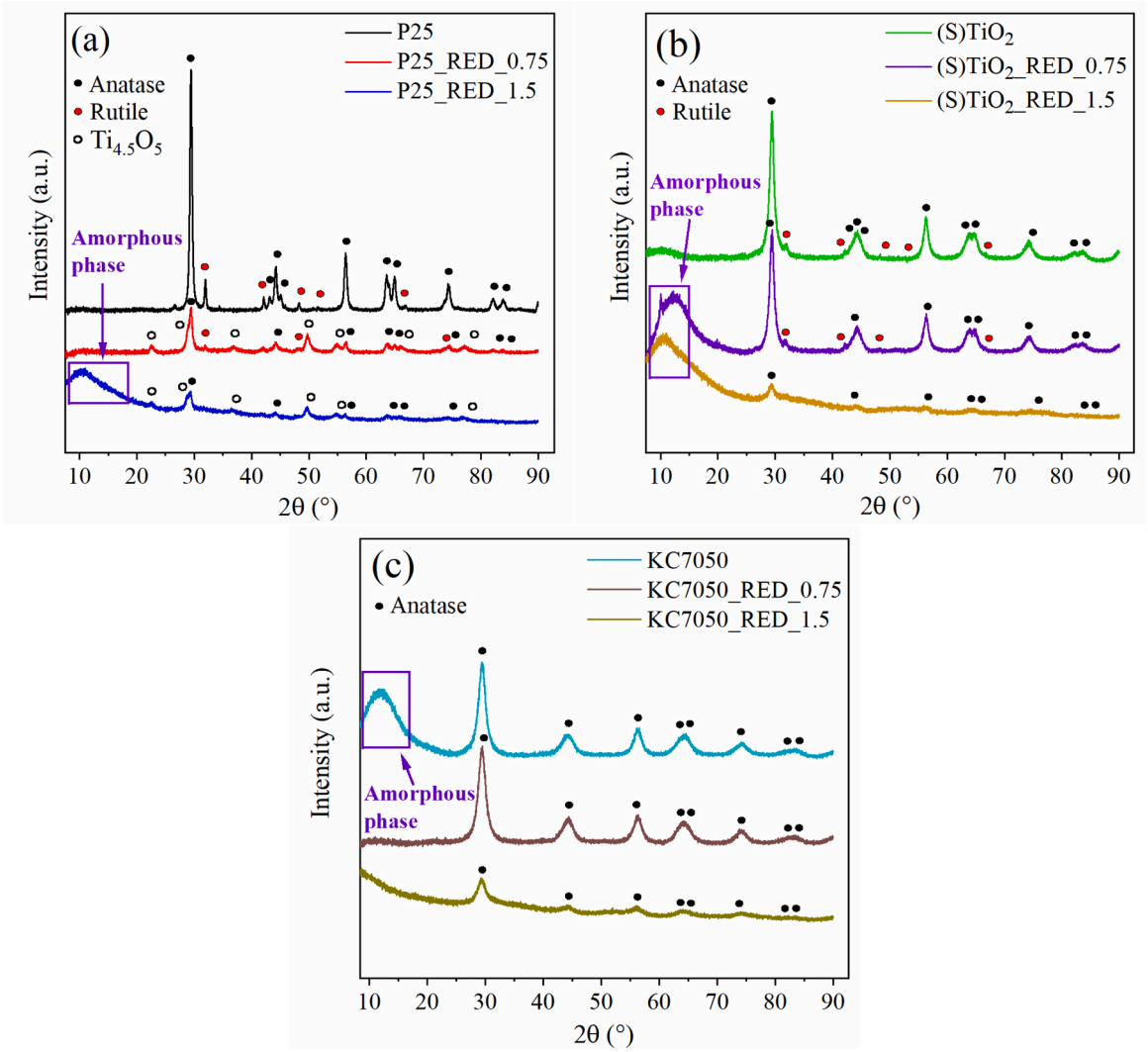

Fig. 1. XRD patterns of photocatalysts based on a) P25, b) (S)TiO_2, and c) KC7050.

process and the formation of defects on the surface of the investigated photocatalysts due to the release of hydrogen during the $NaBH_4$ reduction [41,42]. The mechanism of this reaction can be briefly described by Eq. 1 [43]:

$$NaBH_4 \quad (s) \rightarrow \sum_i solid_i(Na, B, H) + \sum_j gas_j(B, H) \tag{1}$$

In summary, it is clear that in the case of P25 and (S)TiO_2 samples, the $NaBH_4$ reduction led to a decrease in the anatase content and the formation of a large amount of amorphous phase. Furthermore, for commercial P25-based samples, the formation of an intermediate phase $Ti_{4.5}O_5$ was registered, whose appearance and influence on the photocatalytic properties have not been adequately studied. A different situation was observed for KC7050-based samples, where the $NaBH_4$ reduction led to complete degradation of the amorphous phase and the formation of pure anatase, even with lower amounts of $NaBH_4$ reductant used.

From the XRD patterns of the tested materials shown in Fig. 1, the relation between the amount of reductant $NaBH_4$ used in synthesising the photocatalysts and the broadening of the diffraction lanes of anatase and rutile is evident. In particular, it is possible to observe a gradual broadening of the anatase and rutile peaks with increasing amounts of $NaBH_4$ reductant used. This phenomenon corresponds to the decrease in the crystallite size of the anatase and rutile contained in the TiO_2 photocatalysts (Table 3) or also to the existence of oxygen vacancies and Ti^{3+} in the structure of the photocatalysts, the presence of which was later demonstrated by Raman spectroscopy and electron paramagnetic resonance (EPR) [44,45].

Raman spectroscopy represents one of the most efficient techniques to obtain information about the defects caused by microstructural disorders. Fig. 2(a-f) shows the full Raman spectra and their polymorphs for untreated samples of TiO_2 nanomaterials P25, (S)TiO_2, KC7050, and their treated forms subjected to chemical reduction with different amounts of $NaBH_4$ reductant (0.75 and 1.5 g). Based on the depicted spectra of the individual samples, it can be summarized that the Raman modes E_g, E_g, B_{1g}, A_{1g}+B_{1g}, and E_g are noticeable for all studied photocatalysts. These vibrations indicate the presence of the anatase phase in the structure of these samples [46,47]. Furthermore, it is possible to observe the broadening of the characteristic Raman peaks of the investigated samples depending on the gradual addition of the $NaBH_4$ reductant during the synthesis of the photocatalyst, which is connected with the lower crystallinity. In addition to these effects, a hypsochromic shift of the most prominent peak from the initial 137 cm^{-1} in the case of the untreated P25 to the final 152 cm^{-1} for its reduced sample P25_RED_1.5 was detected, as shown in Fig. 2a) and b). A similar trend is also evident for the (S)TiO_2 RED_1.5 (Fig. 2c), d)) and KC7050_RED_1.5 (Fig. 2e), f)) samples. These phenomena correspond to the disintegration of the original TiO_2 lattice and the introduction of the disordered TiO_{2-x} layer [48]. At the same time, this blue shift can be attributed to the existence of oxygen vacancies and Ti^{3+} sites in the structure of the reduced TiO_2 samples, whose presence was partially confirmed by XRD analysis [49].

Table 3
The crystallite size of the investigated TiO_2 samples.

Sample name	Crystallite size		
	Anatase (nm)	Rutile (nm)	$Ti_{4.5}O_5$ (nm)
P25	30	37	-
P25_RED_0.75	10	14	11
P25_RED_1.5	3	-	15
(S)TiO_2	18	20	-
(S)TiO_2 RED_0.75	11	3	-
(S)TiO_2 RED_1.5	3	-	-
KC7050	7	-	-
KC7050_RED_0.75	22	-	-
KC7050_RED_1.5	6	-	-

In order to obtain information on the defect structure in different TiO_2-based precursors and their corresponding reduced forms, an electron paramagnetic resonance measurement was carried out. Fig. 3a) shows the EPR trace of the P25 sample where two characteristic regions for TiO_2-based nanomaterials, arising from different Ti^{3+} defect sites, can be recognized: (1) weak axial resonant line at $g = 1.997$ corresponding to lattice embedded Ti^{3+} sites in anatase phase of TiO_2 and (2) more pronounced peak at $g = 1.967$ which corresponds to Ti^{3+} defects in the crystalline structure of rutile phase, which is in line with previously published work on P25 [50]. These observations point towards the mixed-phase nature of P25 samples, where the majority of Ti^{3+} defects are located on the rutile phase in the sublayer below the surface of the nanoparticles, which is reflected in the larger linewidth. The EPR spectrum of (S)TiO_2 sample, shown in Fig. 3d), contains the axial EPR signature corresponding to Ti^{3+} sites in an anatase crystalline structure with $g_\perp = 1.997$ and $g_{|||} = 1.977$ [51]. Besides that, a small contribution of the surface oxygen-based holes (e.g. Ti-O*) can be observed in the region B < 325 mT, corresponding to the *g*-value of about 2.022. Similar EPR fingerprints are observed in the EPR spectrum of the KC7050 sample shown in Fig. 3e), which points towards the very similar physical nature of both samples from the EPR point of view. Fig. 3a) shows the EPR spectrum of the reduced P25_RED_0.75 sample, which exhibits a broad dispersion signal at $g = 1.934$, characteristic for Ti^{3+} surface exposed sites [52,53]. Besides the wide resonant line, a tiny modulation can be observed at $g = 1.967$, which points towards a small fraction of Ti^{3+} defects in the anatase crystalline structure. Although the EPR signal intensity is not directly proportional to the number of spin-containing defects in the material structure, it can be stated that sample P25_RED_0.75 contains an enormous amount of defects compared to the other two reduced samples (S)TiO_2 _RED_0.75 and KC7050_RED_0.75. As was in the case of the starting materials, reduced samples (S)TiO_2_RED_0.75 and KC7050_RED_0.75 show very similar signatures in the EPR spectra shown in Fig. 3d) and Fig. 3f). EPR spectrum of (S)TiO_2_RED_0.75 shows axial signal corresponding to Ti^{3+} lattice embedded defects in anatase phase with $g_\perp = 1.997$ and $g_{||} = 1.977$ and broad unresolved component at $g = 2.032$ which is interpreted as oxygen-based holes. Similarly, the EPR spectrum of KC7050_RED_0.75 (Fig. 3f)) exhibits an axial signal corresponding to Ti^{3+} defects in anatase crystalline structure with $g_\perp = 1.994$ and $g_{||} = 1.975$ with small contribution oxygen-based holes at $g = 2.026$. In addition, the spectrum is modulated by a broad component that appears as a wide dispersion tail belonging to the Ti^{3+} surface exposed defects.

The EPR spectra of the samples reduced with 1.5 g of $NaBH_4$ reductant indicate a significantly higher degree of reduction than in the previous batch, which is reflected in higher EPR intensity. Nevertheless, the sample P25_RED_1.5, shown in Fig. 3a), shows an almost identical fingerprint as the sample P25_RED_0.75. The EPR envelope is characterized by a broad resonant line positioned at $g = 1.932$, which is typical for Ti^{3+} surface exposed sites, and it is modulated by a weak resonant line at $g = 1.967$, which witnesses a small fraction of Ti^{3+} defects in the anatase crystal lattice. EPR spectra of the samples (S)TiO_2_RED_1.5 and KC7050_RED_1.5 shown in Fig. 3c), and e), respectively, show similar features. In both EPR envelopes dominate a broad line around $g = 1.935$, which is, as mentioned above, interpreted as a surface Ti^{3+} defects. Further, we observe a sharp resonant line at $g = 1.995$, which belongs to Ti^{3+} defects in the anatase crystalline structure. In both EPR envelopes in Fig. 3c) and d) can be recognized another resonant line in the region of B < 325 mT, which corresponds to the g-value of about 2.058, which reflects a small contribution of the surface oxygen-based holes.

To summarize EPR results, it can be concluded that the P25 sample contains a mixture of two phases, anatase and rutile, with rutile being predominantly on the particle surface. The other two commercial samples, (S)TiO_2 and KC7050, are very similar based on the EPR analysis. These similarities are related to the application of sulphate technology, which was utilized to synthesize both nanomaterials [38,54,55]. In both

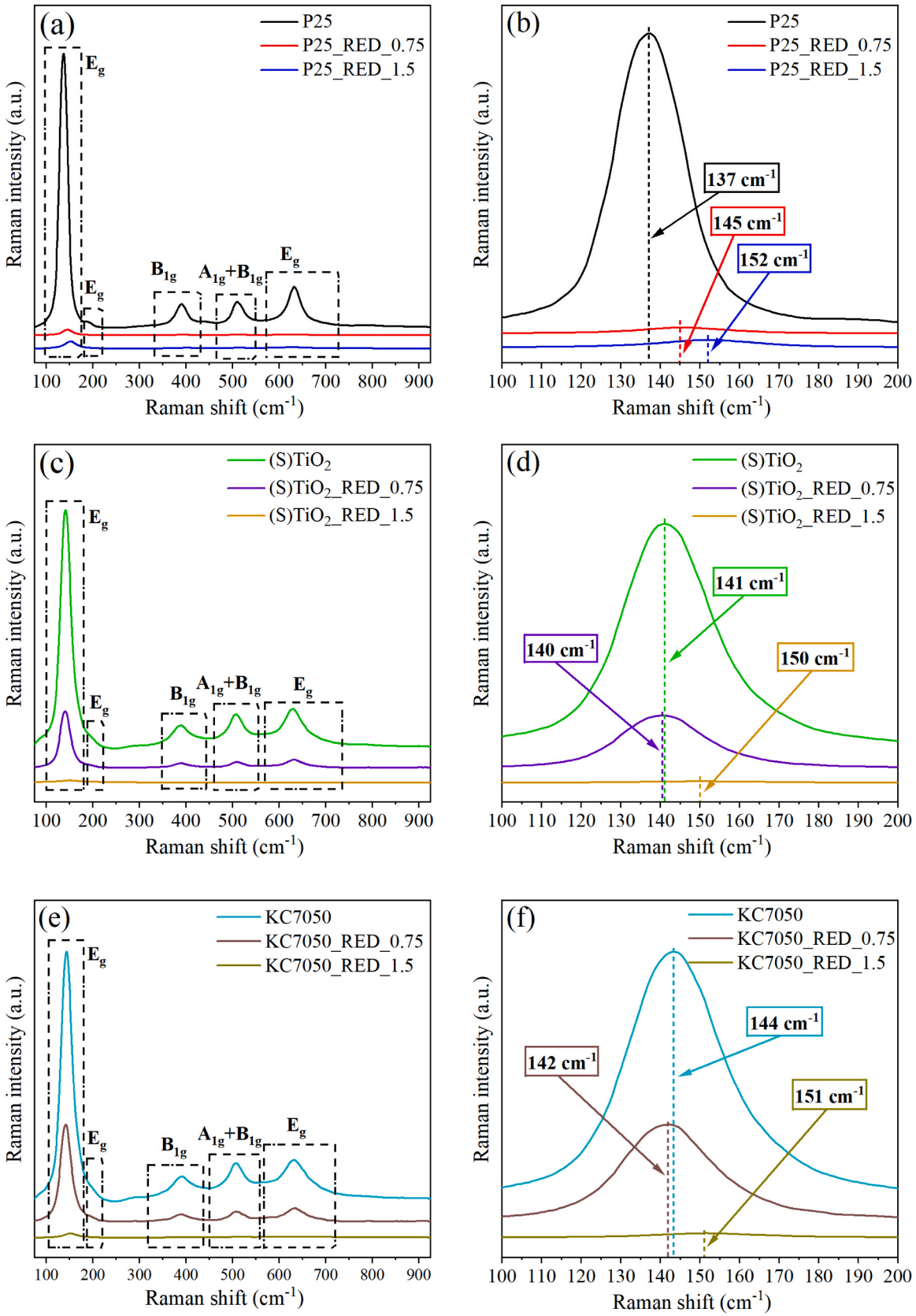

Fig. 2. Raman spectra of the original and reduced photocatalysts: a) full Raman spectra of P25-based photocatalysts, b) zoom of Raman spectra for P25-based samples (Raman shift: 100–200 cm^{-1}), c) full Raman spectra of (S)TiO_2-based photocatalysts, d) zoom of Raman spectra for (S)TiO_2-based samples (Raman shift: 100–200 cm^{-1}), e) full Raman spectra of KC7050-based photocatalysts, and f) zoom of Raman spectra of KC7050-based samples (Raman shift: 100–200 cm^{-1}).

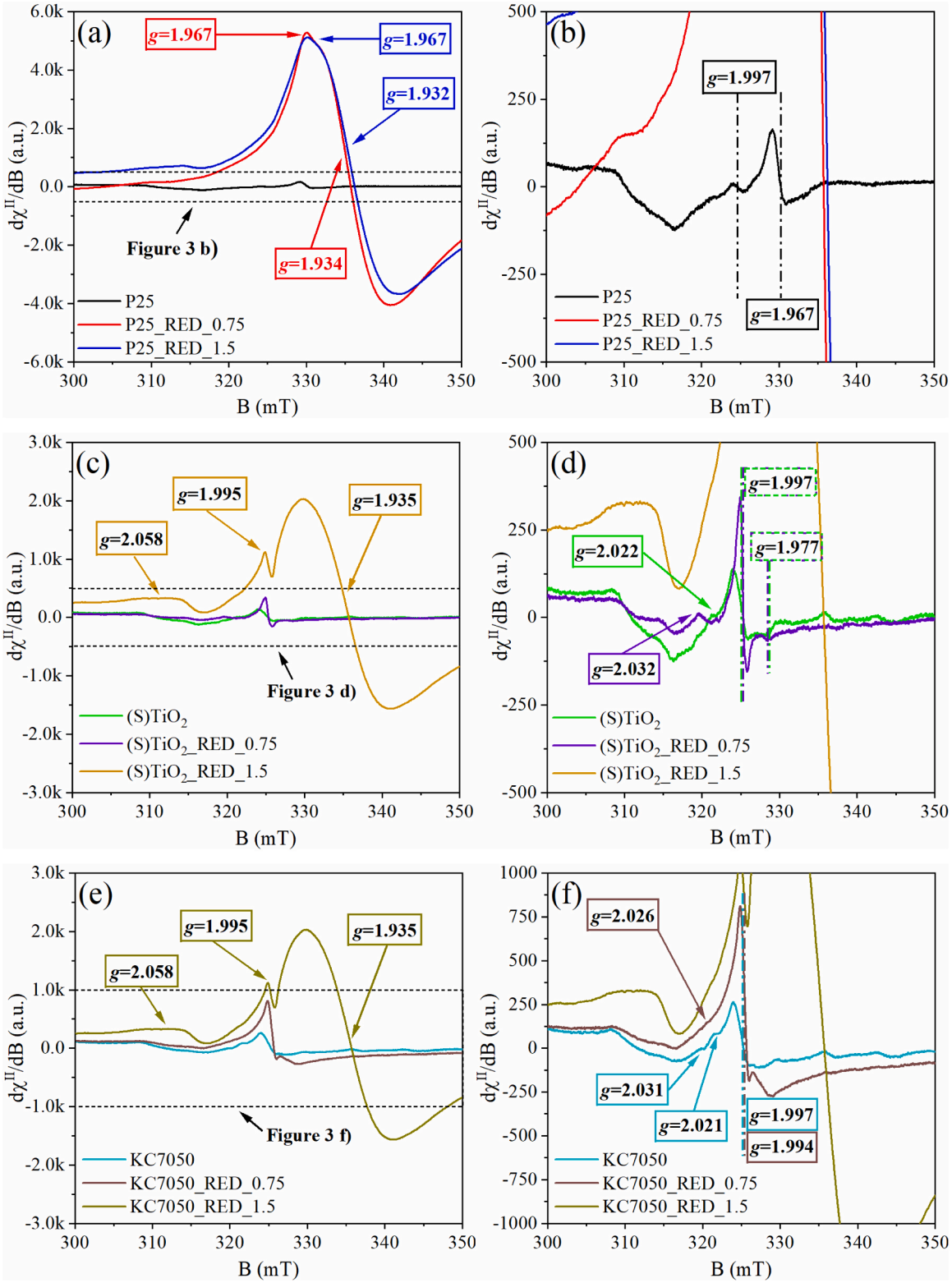

Fig. 3. EPR spectra of the investigated photocatalyst samples: a) full EPR spectra of P25-based samples, b) zoom of EPR spectra for P25-based samples (range of $d\chi^{II}$/dB: −500 – 500), c) full EPR spectra of (S)TiO_2 -based photocatalysts, d) zoom of EPR spectra for (S)TiO_2-based samples (range of $d\chi^{II}$/dB: −500–500), e) full EPR spectra of KC7050-based samples, and f) zoom of EPR spectra for KC7050-based samples (range of $d\chi^{II}$/dB: −1000–1000).

samples, the dominant signal corresponds to the anatase axial signal, reflecting Ti^{3+} defects in the crystal lattice or possibly in some sublayer below the surface. The reduced P25_RED_0.75 sample shows a large number of surface Ti^{3+} defects, which is also consistent with the black colour of the sample. The other two samples reduced with 0.75 g of $NaBH_4$ reductant ((S)TiO_2_RED_0.75 and KC7050_RED_0.75) show very similar signals to their precursors, and apart from very small changes, we observe only an increase in EPR signal intensity, indicating an increase in Ti^{3+} defects during thermal annealing. However, this increase in defect number and subsequent EPR signal is not as strong as in the

previous case, which is also confirmed by the lighter colour of the powder materials. The TiO_2-based samples annealed with 1.5 g of $NaBH_4$ reductant show different characteristics than the photocatalysts reduced with the lower amount of $NaBH_4$ (0.75 g). Only the sample P25_RED_1.5 (Fig. 3a)) shows almost identical EPR fingerprints as the sample P25_RED_0.75 (Fig. 3a)). The remaining two reduced samples (S) TiO_2_RED_1.5 (Fig. 3c)) and KC7050_RED_1.5 (Fig. 3e)) show almost identical EPR fingerprints, suggesting their very similar electronic structure. However, compared to the previous reduced samples ((S) TiO_2_RED_0.75 and KC7050_RED_0.75), they show a much larger representation of surface defects relative to defects localized in the crystal lattice as well as in the total number of defects. As suggested earlier, this also corresponds to much darker shades of grey to black (Fig. S2) than was the case in the previous series.

XPS study of the surface composition of the catalysts treated with the reduction agent ($NaBH_4$) revealed the presence of titanium, oxygen, boron and sodium. Based on the intensities of the photoelectron lines of Ti 2p, O 1 s, B 1 s and Na 1 s, and taking into account the corresponding sensitivity factors, the fractions of each element were calculated, and expressed in atomic percentage (Table 4). The ratio of oxygen to titanium for all tested samples is about 3, a value typically observed for titanium oxide surfaces [56]. Due to the large ionic radius of the Na^+ ions, the sodium content on the surface is relatively high, reaching a maximum of 10% at. Together with the presence of boron atoms, they confirm the presence of the residual reduction agent in the tested materials.

Analysis of Ti 2p photoelectron lines coming from all analysed materials indicates changes in the electron structure of titanium atoms in titanium oxide subjected to the reduction process (Fig. 4). The maximum of the Ti $2p_{3/2}$ component for pure P25 is located at a binding energy of 458.9 eV, which is typical for pure titanium oxide TiO_2 [57]. Regardless of the concentration of the reducing agent to which this starting material was treated, the Ti $2p_{3/2}$ component shifts toward lower binding energies to a value of 458.6 eV (Fig. 4a)). In addition, a rather significant broadening of the Ti $2p_{3/2}$ line profile in the low binding energy region (of about 456–457 eV) can be observed. In the case of pure titanium oxide (S)TiO_2, the maximum of the Ti $2p_{3/2}$ component is located at a binding energy of 458.8 eV (Fig. 4b)), which is within the measurement error range and suggests the presence of a material with a surface structure very close to pure P25. Subjecting this original material to a lower concentration of reducing agent generally does not lead to any changes in its surface structure. On the other hand, treatment of this material with the reducing agent of higher concentration leads to surface chemical changes manifested by a slight shift in the maximum of the Ti $2p_{3/2}$ component to a binding energy of 458.5 eV. The maximum of the Ti $2p_{3/2}$ component for pure KC7050 material lies at a binding energy of 459.2 eV (Fig. 4c)). This value differs slightly from the binding energies observed for pure P25 and (S)TiO_2 samples, indicating minor differences in the surface structure of these materials. Treating the KC7050 with the reducing agent, a gradual shift of the maximum of the Ti $2p_{3/2}$ component to a binding energy value of 458.8 eV is observed, and at high concentrations of the reducing agent the value of the binding energy reaches 458.5 eV.

Table 4
Surface concentrations of elements identified on the surface of TiO_2-based nanomaterials subjected to $NaBH_4$ reduction treatment.

Sample name	Boron (% at.)	Oxygen (% at.)	Titanium (% at.)	Sodium (% at.)
P25_RED_0.75	5	66	20	9
P25_RED_1.5	8	65	19	8
(S)TiO_2 _RED_0.75	2	66	22	10
(S)TiO_2 _RED_1.5	4	69	20	7
KC7050_RED_0.75	1	68	22	9
KC7050_RED_1.5	4	67	21	8

The shift of the Ti $2p_{3/2}$ line observed in all cases of materials by approximately 0.3 eV with respect to the position of the line for the starting materials corresponds to the formation of defects in the structure of titanium oxide on its surface due to the exposure to the reducing agent. The shift in the position of the Ti $2p_{3/2}$ line toward lower binding energy values may account for the partial reduction of Ti^{4+} ions.

The results obtained from the implemented N_2 adsorption-desorption measurements showed that the unmodified photocatalysts, except the commercial TiO_2 P25-based nanomaterials, possessed a higher specific surface area compared to the reduced samples. The highest specific surface area was determined for the sample of the untreated nanomaterial KC7050 (S_{BET} = 262 m^2/g) and the lowest for the unmodified commercial P25 sample (S_{BET} = 54 m^2/g). As shown in Fig. S3, the shape of the N_2 adsorption-desorption isotherms of the tested samples corresponds to type IV according to the BDDT classification (Brunauer-Deming-Deming-Teller), indicating the mesoporous nature of the photocatalysts [58]. According to the data in Table 5, the dependence of the specific surface area and pore volume of the investigated photocatalysts on the amount of $NaBH_4$ reductant used in the reduction process is evident. Specifically, from the measured values, it is possible to observe three different trends. The original and reduced samples of P25 show an increase in the specific surface area with the increasing amounts of $NaBH_4$ reductant used. In particular, the specific surface area of the P25_RED_1.5 sample is almost double that of the original commercial P25 photocatalyst. This increase can be attributed to the formation of pores during the decomposition of the $NaBH_4$ reductant [59], which corresponds to the data in Table 4. In contrast, KC7050-based samples exhibit a different trend. From the measured values, it is possible to observe a decrease in textural parameters (specific surface area, pore volume) with an increasing amount of added $NaBH_4$ reductant. The (S)TiO_2-based samples show a similar trend, respectively a decrease in the textural parameters with increasing amount of $NaBH_4$ reductant, but the (S)TiO_2_RED_1.5 sample also has a negligibly higher specific surface area compared to the reduced sample (S)TiO_2_RED_0.75.

The light absorption and band gap energies of the tested TiO_2-based photocatalysts were determined by UV-Vis diffuse reflectance spectroscopy. Detailed analysis of UV-Vis absorbance spectra (Fig. 5) revealed that all investigated TiO_2 samples exhibited high internal absorption of the crystalline anatase phase, corresponding to large absorption peaks in the range of wavelengths 250–400 nm. Furthermore, treated TiO_2 nanomaterials show a higher absorption ability in the visible region of light spectra than unmodified TiO_2 photocatalysts. This hypothesis was manifested by a striking increase in absorbance in the wavelength range of 400 – 800 nm (Fig. 5). In particular, modified TiO_2 materials based on commercial P25 exhibit the highest absorption of visible light. The extended absorbance of the reduced photocatalysts from the UV to the visible region of the light spectra corresponds to the colour changes of the materials studied (Fig. S2). Specifically, the reduced P25-based samples, (S)TiO_2_RED_1.5, and KC7050_RED_1.5 are significantly darker compared to the photocatalysts in the original state (P25, (S)TiO_2, KC7050), which have retained their white colour. The enhanced absorption of the reduced photocatalysts can be attributed to the effect of blackening of the nanomaterials, associated with the introduction of oxygen vacancies and Ti^{3+} sites on the surface of the synthesized samples and the formation of an amorphous shell over the TiO_2-based crystalline core [60]. The band gap energies of the investigated photocatalysts were calculated using the Kubelka-Munk function (Table 5). The constructed Tauc plots of the studied materials are shown in Fig. S4 in the Supplementary Materials [61]. As expected, all unmodified TiO_2 samples have band gap energy values in the range of binding energies between 3.24 and 3.34 eV, consistent with the band gap energy of pure TiO_2 [62]. The most significant extension of the band gap is particularly evident for the reduced P25 samples. The lowest band gap energy value of 3.21 eV was determined for the reduced sample (S)TiO_2_RED_0.75. In contrast, all reduced samples of photocatalysts, except the mentioned sample (S)TiO_2_RED_0.75, possess higher band

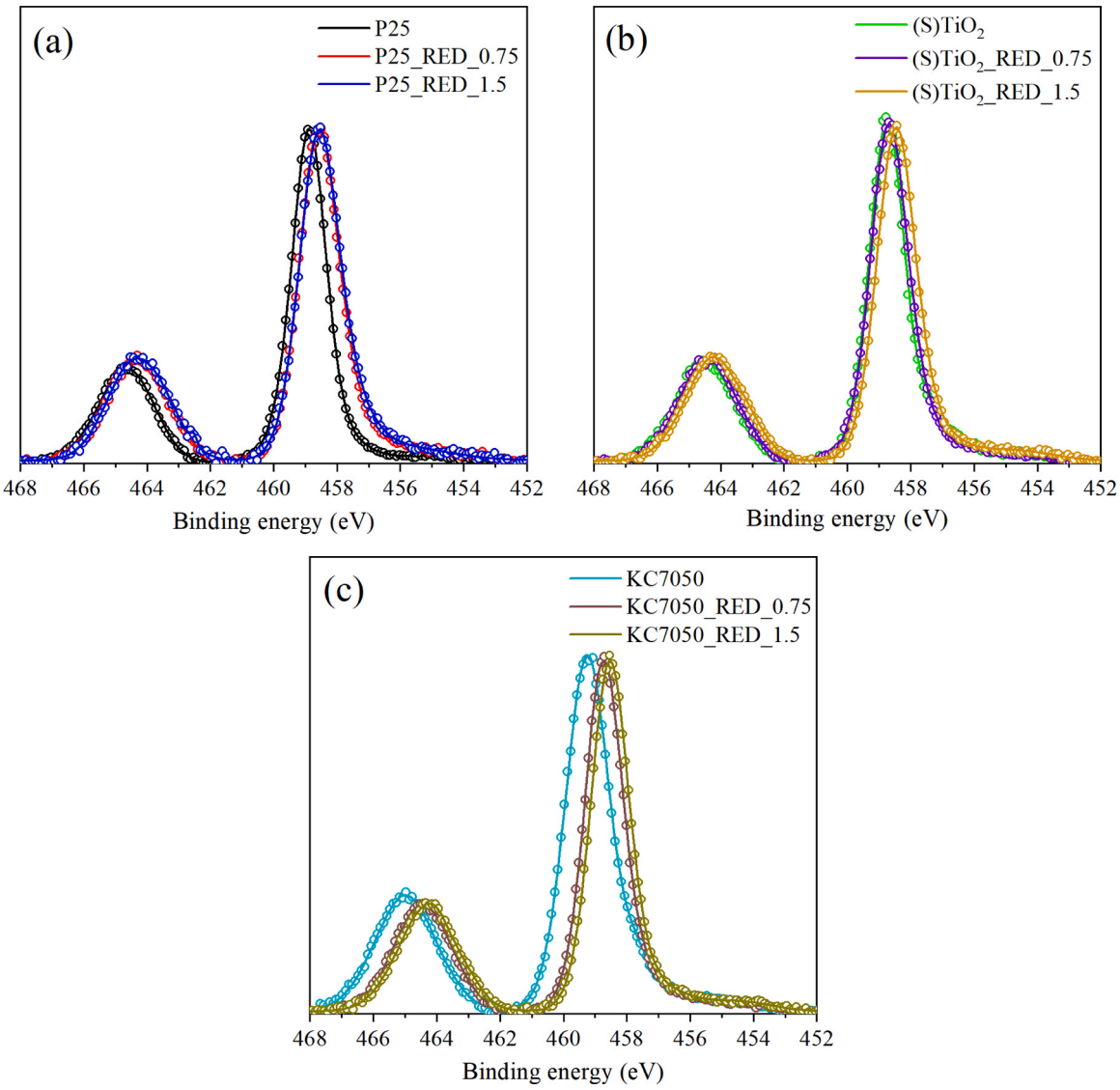

Fig. 4. XPS Ti 2p spectra of photocatalysts based on a) P25, b) (S)TiO_2, and c) KC7050.

Table 5
Specific surface area, pore volumes, and band gap energies of the tested TiO_2 photocatalysts.

Sample name	S_{BET} ($m^2/g_{cat.}$)	V_{total} * ($cm^3/g_{cat.}$)	V^{**}_{micro} ($cm^3/g_{cat.}$)	V^{***}_{meso} ($cm^3/g_{cat.}$)	E_g (eV)
P25	54	0.40	0.02	0.38	3.24
P25_RED_0.75	85	0.28	0.03	0.25	3.48
P25_RED_1.5	90	0.79	0.03	0.76	3.54
(S)TiO_2	224	0.33	0.07	0.26	3.34
(S)TiO_2 _RED_0.75	162	0.32	0.06	0.26	3.21
(S)TiO_2 _RED_1.5	172	0.24	0.06	0.18	3.48
KC7050	262	0.29	0.09	0.20	3.29
KC7050_RED_0.75	196	0.27	0.07	0.20	3.32
KC7050_RED_1.5	165	0.21	0.06	0.15	3.42

* Total pore volume determined by the single point from the N_2 adsorption isotherms at relative pressures $p/p_0 = 0.95$.
** Volume of micropores calculated using the Dubinin-Radushkevich equation.
*** Volume of mesopores estimated from the difference between V_{total} and V_{micro}.

gap energy values compared to the TiO_2-based samples in the original state. This increase can be attributed to the decrease in the size of the anatase and rutile crystallites, as demonstrated by the XRD data in Table 3.

3.2. Photocatalytic activity of the investigated photocatalysts

The photocatalytic activity of TiO_2-based samples was evaluated by measurements of the photocatalytic reduction of CO_2 carried out in the presence of a UVC pen-ray lamp (λ_{max} = 254 nm). Individual time dependences of UVC irradiation on product yields during photocatalytic reduction of CO_2 are shown in the Supplementary Materials (Fig. S5 and S6).

Based on the product yields after 7 h of UVC irradiation depicted in Fig. 6, the relation between the photocatalytic activity of the investigated samples and the amount of $NaBH_4$ reductant (degree of TiO_2 reduction) used during the synthesis of the photocatalysts is evident. In particular, it is possible to observe an enhanced photocatalytic performance of reduced TiO_2-based photocatalysts with higher amount (1.5 g) of the $NaBH_4$ reductant. As shown in Fig. 6, all P25, (S)TiO_2, and KC7050 nanomaterials reduced with a lower amount of $NaBH_4$ reductant (0.75 g) exhibit significantly lower photocatalytic activity than the original samples. In contrast, TiO_2-based photocatalysts reduced with 1.5 g of $NaBH_4$ show an opposite trend. The photocatalytic activity of these samples is significantly higher compared to the TiO_2-based

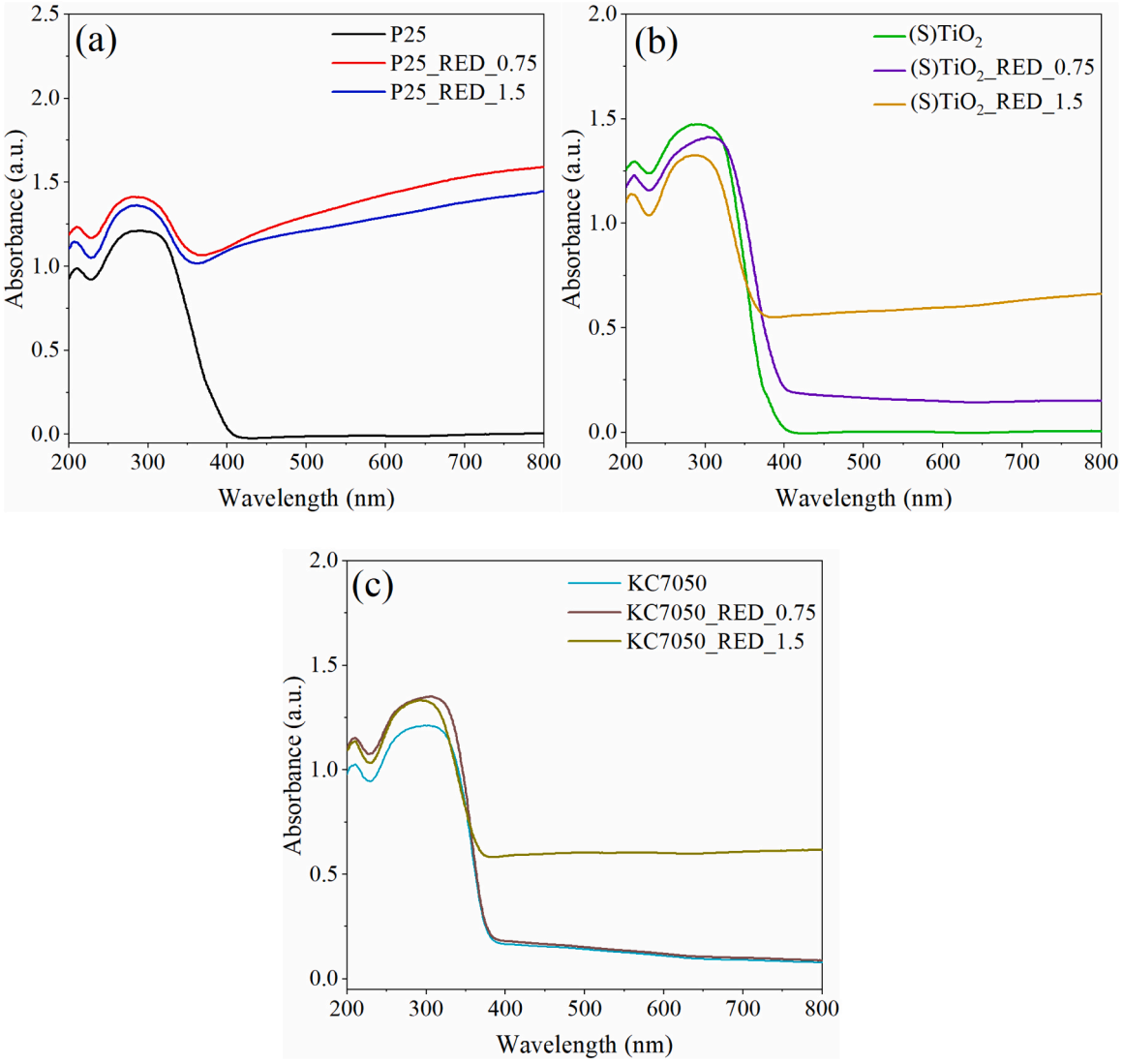

Fig. 5. UV-Vis absorption patterns of the investigated samples based on a) P25, b) (S)TiO_2, and c) KC7050.

samples reduced with the lower amount of $NaBH_4$ (0.75 g). Sample KC7050, reduced with 1.5 g of $NaBH_4$ reducing agent, exhibited the highest product yields, demonstrating its superior photocatalytic activity among all the investigated photocatalysts.

Regarding the photocatalytic activity for a CO_2 reduction, the focus should be on the carbon monoxide and methane yields formed as the main products of the photocatalytic reduction of CO_2 reaction. The formation of these products can be described by Eqs. 2 and 3.

$$CO_2 + 2H^+ + 2e^- \rightarrow CO + H_2O \quad (2)$$

$$CO_2 + 8H^+ + 8e^- \rightarrow CH_4 + 2H_2O \quad (3)$$

According to the data shown in Fig. 6a) and b), it can be stated that the highest photocatalytic activity for a CO_2 reduction exhibits the treated sample KC7050_RED_1.5, while the modified sample KC7050_RED_0.75 shows the lowest photocatalytic performance.

In addition to CH_4 and CO, high H_2 yields were also observed (Fig. 6c). However, the evolution of H_2 is linked to a side reaction of water splitting, which is associated with the oxidation of water and, therefore, the hydrogen formation (Eq. 4).

$$2H^+ + 2e^- \rightarrow H_2 \quad (4)$$

All investigated TiO_2-based photocatalyst samples were measured at least 3 times, implying that the same batch (0.1 g of photocatalyst with 100 ml of 0.2 M NaOH) was used each time and again was saturated with CO_2. Therefore, based on the photocatalytic experiments performed, it can be summarized that the results obtained were reproducible and thus the stability of the tested photocatalyst samples was verified. Measurement errors were in the range of 5% (Fig. 6).

Based on the photocatalytic reduction of CO_2 results, it is remarkable that the prepared samples of all TiO_2-based photocatalysts reduced with 0.75 g of $NaBH_4$ (P25_RED_0.75, (S)TiO_2_RED_0.75, KC7050_RED_0.75) exhibit much lower photocatalytic activity for a CO_2 reduction than the samples of untreated TiO_2 nanomaterials. The low photocatalytic activity could be explained by two factors. First, samples (S)TiO_2_RED_0.75 and KC7050_RED_0.75 show obvious signs of insufficient $NaBH_4$ reduction, which was reflected by the light colour of these samples and thus the presence of just minor amount of introduced defects. Second, the SEM-EDX maps demonstrate that all TiO_2-based samples reduced with 0.75 g of the $NaBH_4$ reductant possess a high sodium content embedded on the surface of these photocatalysts. Thus, the positive effect of Ti^{3+} defects and oxygen vacancies on the photocatalytic activity was suppressed due to undesirable surface recombination induced by sodium ions, which act as recombination centers and thereby impair the photocatalytic activity of these photocatalyst samples [13,63–65]. The SEM-EDX images of the P25_RED_0.75, (S)

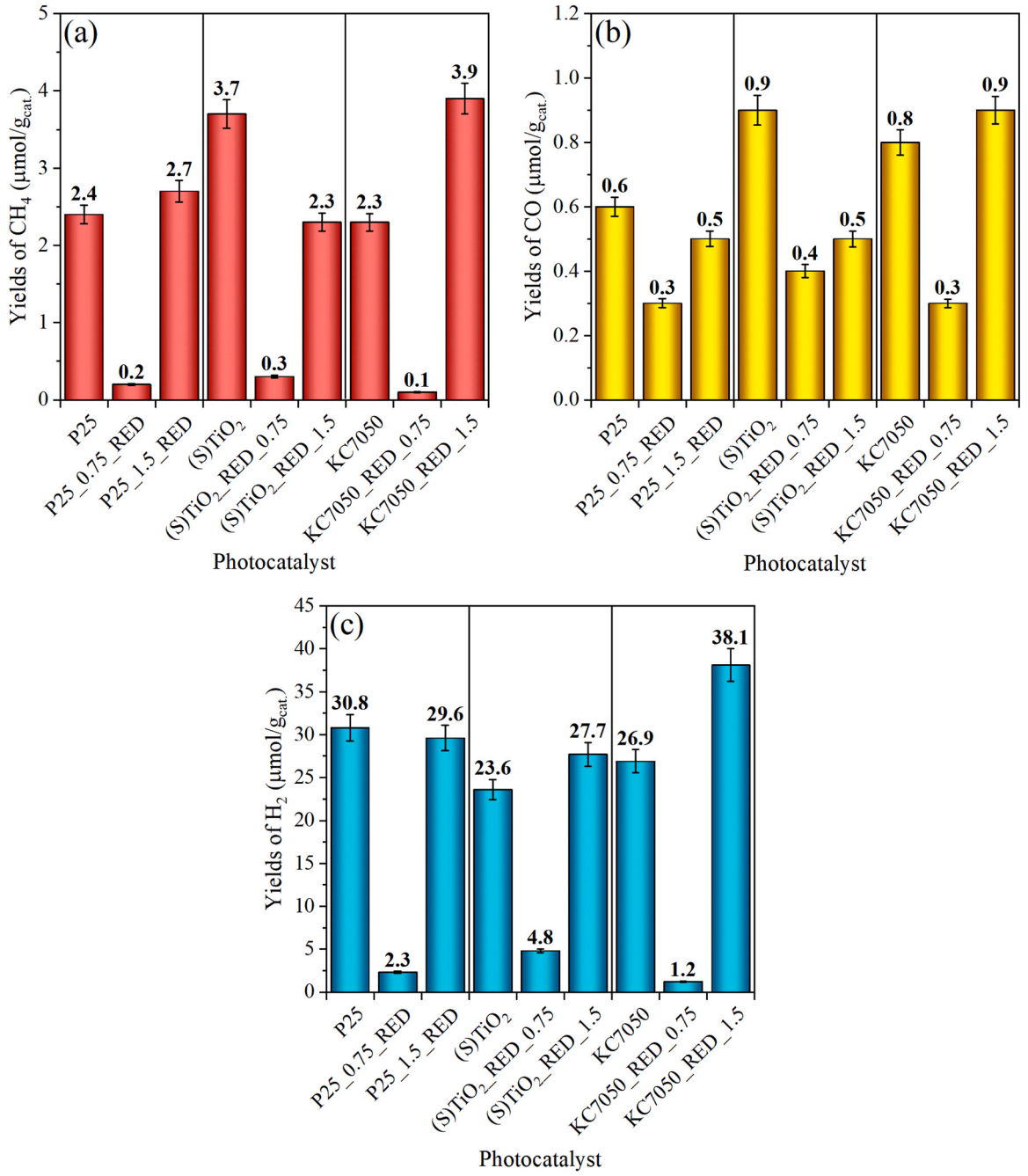

Fig. 6. Yields of a) CH_4, b) CO, and c) H_2 with the marked error bars after 7 h of UVC irradiation ($\lambda_{max.}$ = 254 nm) in the presence of the investigated photocatalysts.

TiO_2_RED_0.75, and KC7050_RED_0.75 are shown in Fig. S7 in the Supplementary Materials.

In contrast, the investigated samples of TiO_2-based nanomaterials treated with a higher amount of $NaBH_4$ reductant (1.5 g) showed the opposite trend, an increase in the photocatalytic activity for a CO_2 reduction compared to the set of samples reduced with 0.75 g of $NaBH_4$ reductant.

Based on the results obtained from the photocatalytic experiments performed with the treated samples P25_RED_1.5 and (S)TiO_2_RED_1.5, it was surprising that the P25_RED_1.5 exhibited only negligibly higher photocatalytic efficiency compared to the original sample P25 and the photocatalyst (S)TiO_2_RED_1.5 showed even lower photocatalytic activity than the original sample (S)TiO_2. However, a more thorough investigation of the XRD, EPR, and Raman spectra of the mentioned samples will help to clarify these trends in photocatalytic activity. Although at first glance it is obvious that both photocatalyst samples contained a significant amount of Ti^{3+} sites and oxygen vacancies, as demonstrated by the results of the EPR analysis and Raman spectroscopy, their positive effect on the photocatalytic activity was largely suppressed by the presence of a significant amount of amorphous phase formed as a result of $NaBH_4$ reduction with 1.5 g of $NaBH_4$ reductant. In addition, both photocatalysts P25_RED_1.5 and (S)TiO_2_RED_1.5 show not only the low representation of the crystalline phase in the form of anatase and $Ti_{4.5}O_5$ in the case of sample P25_RED_1.5, but also very low crystallinity of the crystalline anatase phase. Based on the obtained XRD results of these samples, it can be stated that the crystallite size of the crystalline anatase phase dramatically decreased from the original 30.3 nm to 3.0 nm in the case of reduced sample of P25 (P25_RED_1.5) and from the initial 18.4 nm to 3.0 nm for the reduced sample (S)TiO_2_RED_1.5. This factor can significantly affects the resulting

photocatalytic activity of these tested nanomaterial samples [66]. The negative effect of the low crystallinity of TiO_2 photocatalysts on their photocatalytic properties was observed, for example, by Xie et al. [67], who confirmed the increasing photocatalytic activity with a gradual increase in the crystallite size of the prepared TiO_2 photocatalysts. The same claim was indirectly supported by Liu et al. [68], who reported that the high crystallinity of Ti^{3+} self-doped TiO_2 photocatalysts considerably enhances their photocatalytic activity.

The highest photocatalytic activity for a CO_2 reduction exhibited the sample KC7050_RED_1.5. The enhanced photocatalytic efficiency of this sample can be elucidated by detailed analysis of the XRD, EPR, and Raman spectroscopy results, which confirmed not only the successful transformation of the original mixed anatase/amorphous phase into a pure anatase as a result of the $NaBH_4$ reduction with 1.5 g of $NaBH_4$ reductant, but also the formation of a disordered surface layer consisting of Ti^{3+} defects and oxygen vacancies. The positive effect of the embedded Ti^{3+} sites and oxygen vacancies is mainly due to the introduction of disordered surface states into the photocatalyst band gap, which is reflected in improved irradiation absorption and also suppression of undesired charge recombination due to the trapping of generated electrons in defects states [44,69]. The positive effect of oxygen vacancies and Ti^{3+} sites is also highlighted by Sorcar et al. [70] and Xu et al. [71], who emphasize in their studies the effectiveness of $NaBH_4$ reduction, associated with the decomposition of the original sodium borohydrate and the release of H_2, in successfully forming the oxygen vacancies and Ti^{3+} sites, the presence of which even resulted in an enhanced charge separation ability, ultimately contributing to the elevated yields of CO and CH_4 as the main products of the photocatalytic reduction of CO_2. The plausible mechanism of the photocatalytic reduction of CO_2 over the KC7050_RED_1.5 photocatalyst sample illustrates the Fig. 7.

4. Conclusions

In this work, the photocatalytic activity of Ti^{3+} self-doped TiO_2-based photocatalysts was assessed by the photocatalytic reduction of CO_2. The investigated photocatalyst samples were synthesized by a simple $NaBH_4$ reduction method that included mixing and grinding commercial TiO_2 powders with $NaBH_4$ reductant, followed by calcination in an argon atmosphere at 350 °C. As titania sources, three different commercial TiO_2-based nanomaterials (P25, (S)TiO_2, and KC7050) were used. In order to study the effect of the amount of $NaBH_4$ reductant on the changes in the physical-chemical and photocatalytic properties of the synthesized TiO_2-based photocatalysts, selected commercial TiO_2 samples (2 g) were reduced with 0.75 and 1.5 g of $NaBH_4$ reducing agent.

Based on the obtained results, the strong dependence of the photocatalytic activity for a CO_2 reduction of the tested photocatalyst samples on the phase composition, the defect structure, and the presence of Na ions was observed. The performed photocatalytic experiments demonstrated that the resulting photocatalytic activity of the set of TiO_2-based samples reduced with a lower amount (0.75 g) of $NaBH_4$ is significantly lower compared to the original non-reduced samples. This is due to a low degree of reduction with $NaBH_4$, which was reflected by the low abundance of Ti^{3+} sites and oxygen vacancies on the surface of the prepared photocatalysts and incorporation of sodium ions into the low-defective structure of TiO_2.

In contrast, samples reduced with 1.5 g of $NaBH_4$ reductant (namely P25_RED_1.5 and KC7050_RED_1.5) show an opposite trend compared to those reduced with 0.75 g of $NaBH_4$ reductant. From the results obtained, it can be summarized that the photocatalytic performance of these samples is mainly affected by their crystallinity (content of amorphous/crystalline phases) and contents of Ti^{3+} defects and oxygen vacancies.

The highest photocatalytic efficiency for a CO_2 reduction exhibited the reduced sample KC7050_RED_1. The enhanced photocatalytic activity of this sample is assigned to its preserved crystalline structure after $NaBH_4$ reduction, and the presence of the disordered TiO_{2-x} layer containing a large number of Ti^{3+} defects and oxygen vacancies, which are responsible for the introduction of disordered surface states and thus contribute to the improvement of light absorption and suppression of charge recombination.

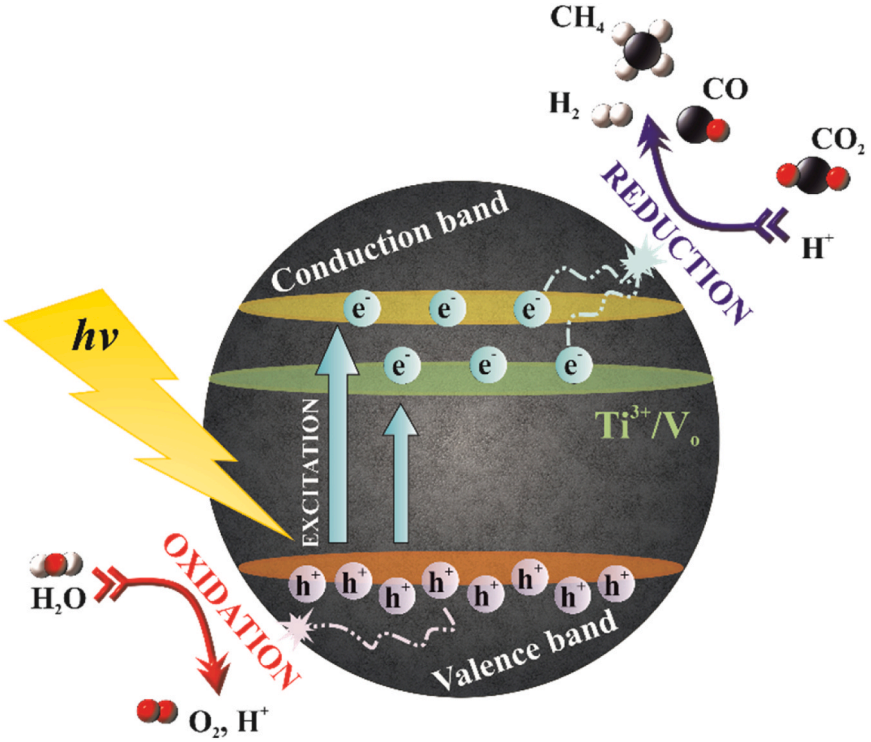

Fig. 7. Plausible mechanism of the photocatalytic reduction of CO_2 over the KC7050_RED_1.5 sample.

In conclusion, our research provides an important insight into the efficiency of TiO_2 photocatalysts in CO_2 reduction highlighting the importance of suitable combination of catalyst crystallinity and defect engineering (Ti^{3+} self-doping).

CRediT authorship contribution statement

Rudolf Ricka: Investigation, Writing – original draft, Methodology, Writing – review & editing. **Agnieszka Wanag:** Investigation, Methodology, Writing – original draft. **Ewelina Kusiak-Nejman:** Investigation, Methodology, Writing – original draft. **Dariusz Moszyński:** Investigation, Methodology. **Miroslava Filip Edelmannová:** Investigation, Methodology, Writing – original draft. **Martin Reli:** Investigation, Methodology, Writing – original draft. **Zdeněk Baďura:** Investigation, Methodology, Writing – original draft. **Giorgio Zoppellaro:** Investigation, Methodology. **Radek Zbořil:** Conceptualization, Methodology, Visualization, Writing – review & editing. **Antoni W. Morawski:** Conceptualization, Investigation, Methodology, Writing – original draft. **Kamila Kočí:** Conceptualization, Writing – original draft, Writing – review & editing, Methodology.

Declaration of Competing Interest

The authors declare that they have no known competing financial interests or personal relationships that could have appeared to influence the work reported in this paper.

Data Availability

Data will be made available on request.

Acknowledgements

The work was financially supported by the Large Research Infrastructure ENREGAT (project No. LM2023056), Norway Grants 2014–2021 via the National Centre for Research and Development (grant No. NOR/POLNORCCS/PhotoRed/0007/2019-00), Czech Science Foundation GA CR 21-24268K, European Union's Horizon 2020 project SAN4Fuel (Grant No. HORIZON-WIDERA-2021-ACCESS-03–01: 101079384). The authors also acknowledge the support by European Union under the REFRESH - Research Excellence For Region Sustainability and High-tech Industries project number, CZ.10.03.01/00/22_003/0000048 via the Operational Programme Just Transition. and the grant program "Support for Science and Research in the Moravia-Silesia Region 2022″ (RRC/12/2022). Z. Baďura acknowledges support from project "APPROACH" No 101120397, HORIZON-WIDERA-2022-TALENTS. The authors would also like to thank A. Martaus for performing the XRD analysis, K. M. Górecki for providing the SEM-EDX images of the investigated samples, and M. Ritz for Raman spectroscopy measurements.

Appendix A. Supporting information

Supplementary data associated with this article can be found in the online version at doi:10.1016/j.jcou.2024.102701.

References

[1] H. Shen, T. Peppel, J. Strunk, Z. Sun, Photocatalytic reduction of CO_2 by metal-free-based materials: recent advances and future perspective, Sol. RRL 4 (8) (2020) 1900546, https://doi.org/10.1002/solr.201900546.
[2] D.o.E.a.S.A. United Nations, Population Division, World Population Prospects 2022: Summary of Results, 2022.
[3] E. Ganivet, Growth in human population and consumption both need to be addressed to reach an ecologically sustainable future, Environ., Dev. Sustain. 22 (6) (2020) 4979–4998, https://doi.org/10.1007/s10668-019-00446-w.
[4] A. Balali, A. Yunusa-Kaltungo, R. Edwards, A systematic review of passive energy consumption optimisation strategy selection for buildings through multiple criteria decision-making techniques, Renew. Sustain. Energy Rev. 171 (2023) 113013, https://doi.org/10.1016/j.rser.2022.113013.
[5] K. Prabhu Teja, V. Shetty Kodialbail, Visible light mediated photocatalytic reduction of CO_2 to non-fossil fuel and valuable products by polyaniline-TiO_2 nanocomposites, Arab. J. Sci. Eng. 47 (5) (2022) 6591–6603, https://doi.org/10.1007/s13369-021-06450-5.
[6] W. Wang, L. Wang, W. Su, Y. Xing, Photocatalytic CO_2 reduction over copper-based materials: a review, J. CO_2 Util. 61 (2022) 102056, https://doi.org/10.1016/j.jcou.2022.102056.
[7] A. Bratovčić, V. Tomašić, Design and development of photocatalytic systems for reduction of CO_2 into valuable chemicals and fuels, Processes 11 (5) (2023) 1433, https://doi.org/10.3390/pr11051433.
[8] T. Inoue, A. Fujishima, S. Konishi, K. Honda, Photoelectrocatalytic reduction of carbon dioxide in aqueous suspensions of semiconductor powders, Nature 277 (5698) (1979) 637–638, https://doi.org/10.1038/277637a0.
[9] B.T. Barrocas, N. Ambrožová, K. Kočí, Photocatalytic reduction of carbon dioxide on TiO_2 heterojunction photocatalysts-a review, Materials 15 (3) (2022) 967, https://doi.org/10.3390/ma15030967.
[10] N. Nandal, S.L. Jain, A review on progress and perspective of molecular catalysis in photoelectrochemical reduction of CO_2, Coord. Chem. Rev. 451 (2022) 214271, https://doi.org/10.1016/j.ccr.2021.214271.
[11] A.W. Morawski, K. Ćmielewska, E. Kusiak-Nejman, P. Staciwa, J. Kapica-Kozar, E. Ekiert, I. Pełech, U. Narkiewicz, The influence of the addition of carbon spheres on photoactivity of TiO_2 and ZnO in CO_2 reduction process, J. CO_2 Util. 75 (2023) 102553, https://doi.org/10.1016/j.jcou.2023.102553.
[12] R.R. Ikreedeegh, M. Tahir, A critical review in recent developments of metal-organic-frameworks (MOFs) with band engineering alteration for photocatalytic CO_2 reduction to solar fuels, J. CO_2 Util. 43 (2021) 101381, https://doi.org/10.1016/j.jcou.2020.101381.
[13] M. Madi, M. Tahir, Z.Y. Zakaria, 2D/2D V2C mediated porous g-C_3N_4 heterojunction with the role of monolayer/multilayer MAX/MXene structures for stimulating photocatalytic CO_2 reduction to fuels, J. CO_2 Util. 65 (2022) 102238, https://doi.org/10.1016/j.jcou.2022.102238.
[14] D. Ješić, D. Lašič Jurković, A. Pohar, L. Suhadolnik, B. Likozar, Engineering photocatalytic and photoelectrocatalytic CO_2 reduction reactions: Mechanisms, intrinsic kinetics, mass transfer resistances, reactors and multi-scale modelling simulations, Chem. Eng. J. 407 (2021) 126799, https://doi.org/10.1016/j.cej.2020.126799.
[15] H. Yin, J. Li, New insight into photocatalytic CO_2 conversion with nearly 100% CO selectivity by CuO-Pd/H_xMoO_{3-y} hybrids, Appl. Catal. B: Environ. 320 (2023) 121927, https://doi.org/10.1016/j.apcatb.2022.121927.
[16] J. Schneider, M. Matsuoka, M. Takeuchi, J. Zhang, Y. Horiuchi, M. Anpo, D. W. Bahnemann, Understanding TiO_2 photocatalysis: mechanisms and materials, Chem. Rev. 114 (19) (2014) 9919–9986, https://doi.org/10.1021/cr5001892.
[17] H. Eidsvåg, S. Bentouba, P. Vajeeston, S. Yohi, D. Velauthapillai, TiO_2 as a photocatalyst for water splitting—an experimental and theoretical review, Molecules 26 (6) (2021) 1687, https://doi.org/10.3390/molecules26061687.
[18] X. Qiu, Z. Wan, M. Pu, X. Xu, Y. Ye, C. Hu, Synthesis and photocatalytic activity of Pt-deposited TiO_2 nanotubes (TNT) for rhodamine B degradation, Front. Chem. 10 (2022), https://doi.org/10.3389/fchem.2022.922701.
[19] V. Verma, M. Al-Dossari, J. Singh, M. Rawat, M.G.M. Kordy, M. Shaban, A review on green synthesis of TiO_2 NPs: photocatalysis and antimicrobial applications, Polymers 14 (7) (2022) 1444, https://doi.org/10.3390/polym14071444.
[20] S. Perera, R. Mariano, K. Vu, N. Nijem, O. Seitz, Y. Chabal, K. Balkus, Hydrothermal synthesis of graphene-TiO_2 nanotube composites with enhanced photocatalytic activity, ACS Catal. 2 (2012) 949–956, https://doi.org/10.1021/cs200621c.
[21] H. Rasouli, F. Jafarpisheh, M. Ghorbanpour, Synthesis and characterization of Sn-doped TiO_2 nanoparticles and the evaluation of their Photocatalytic performance under Vis-lights, J. Water Environ. Nanotechnol. 7 (4) (2022) 344–350, https://doi.org/10.22090/jwent.2022.04.001.
[22] L. Zhang, M. Jaroniec, Toward designing semiconductor-semiconductor heterojunctions for photocatalytic applications, Appl. Surf. Sci. 430 (2018) 2–17, https://doi.org/10.1016/j.apsusc.2017.07.192.
[23] L. Kong, Z. Jiang, C. Wang, F. Wan, Y. Li, L. Wu, J.F. Zhi, X. Zhang, S. Chen, Y. Liu, Simple ethanol impregnation treatment can enhance photocatalytic activity of TiO_2 nanoparticles under visible-light irradiation, 8, ACS Appl. Mater. Interfaces 7 (14) (2015) 7752, https://doi.org/10.1021/acsami.5b00888.
[24] L. Andronic, A. Enesca, Black TiO_2 synthesis by chemical reduction methods for photocatalysis applications, Front. Chem. 8 (2020), https://doi.org/10.3389/fchem.2020.565489.
[25] X. Chen, L. Liu, P.Y. Yu, S.S. Mao, Increasing solar absorption for photocatalysis with black hydrogenated titanium dioxide nanocrystals, Science 331 (6018) (2011) 746–750, https://doi.org/10.1126/science.1200448.
[26] J. Li, E.-H. Wu, J. Hou, P. Huang, Z. Xu, Y. Jiang, Q.-S. Liu, Y.-Q. Zhong, A facile method for the preparation of black TiO_2 by Al reduction of TiO_2 and their visible light photocatalytic activity, RSC Adv. 10 (57) (2020) 34775–34780, https://doi.org/10.1039/D0RA06784A.
[27] Y. Chai, Y. Kong, M. Lin, W. Lin, J. Shen, J. Long, R. Yuan, W. Dai, X. Wang, Z. Zhang, Metal to non-metal sites of metallic sulfides switching products from CO to CH_4 for photocatalytic CO_2 reduction, Nat. Commun. 14 (1) (2023) 6168, https://doi.org/10.1038/s41467-023-41943-x.
[28] A. Bilal, K. Bilal Ahmad, B. Raieesa, Perspective chapter: black titania – from synthesis to applications, in: B. Bochra (Ed.), Updates on Titanium Dioxide, IntechOpen, Rijeka, 2023, p. Ch. 2.

[29] M.U. Azam, M. Tahir, M. Umer, B. Tahir, N. Shehzad, M. Siraj, In-situ synthesis of $TiO_2/La_2O_2CO_3$/rGO composite under acidic/basic treatment with La^{3+}/Ti^{3+} as mediators for boosting photocatalytic H_2 evolution, Int. J. Hydrog. Energy 44 (42) (2019) 23669–23688, https://doi.org/10.1016/j.ijhydene.2019.07.085.

[30] M. Umer, M. Tahir, M.U. Azam, B. Tahir, M. Musaab, Self-doped Ti^{3+} mediated TiO_2/In_2O_3/SWCNTs heterojunction composite under acidic/basic heat medium for boosting visible light induced H_2 evolution, Int. J. Hydrog. Energy 44 (26) (2019) 13466–13479, https://doi.org/10.1016/j.ijhydene.2019.04.020.

[31] R. Nawaz, H. Ullah, A.A.J. Ghanim, M. Irfan, M. Anjum, S. Rahman, S. Ullah, Z. Abdel Baki, V. Kumar Oad, Green synthesis of ZnO and black TiO_2 materials and their application in photodegradation of organic pollutants, ACS Omega 8 (39) (2023) 36076–36087, https://doi.org/10.1021/acsomega.3c04229.

[32] Y.H. Hu, A highly efficient photocatalyst—hydrogenated black TiO_2 for the photocatalytic splitting of water, Angew. Chem. Int. Ed. 51 (50) (2012) 12410–12412, https://doi.org/10.1002/anie.201206375.

[33] C.C. Wang, P.H. Chou, Effects of various hydrogenated treatments on formation and photocatalytic activity of black TiO_2 nanowire arrays, Nanotechnology 27 (32) (2016) 325401, https://doi.org/10.1088/0957-4484/27/32/325401.

[34] G. Zhu, Y. Shan, T. Lin, W. Zhao, J. Xu, Z. Tian, H. Zhang, C. Zheng, F. Huang, Hydrogenated blue titania with high solar absorption and greatly improved photocatalysis, Nanoscale 8 (8) (2016) 4705–4712, https://doi.org/10.1039/C5NR07953E.

[35] V. Kumaravel, S. Rhatigan, S. Mathew, M.C. Michel, J. Bartlett, M. Nolan, S. J. Hinder, A. Gascó, C. Ruiz-Palomar, D. Hermosilla, S.C. Pillai, Mo doped TiO_2: impact on oxygen vacancies, anatase phase stability and photocatalytic activity, J. Phys.: Mater. 3 (2) (2020) 025008, https://doi.org/10.1088/2515-7639/ab749c.

[36] T.S. Rajaraman, S.P. Parikh, V.G. Gandhi, Black TiO_2: a review of its properties and conflicting trends, Chem. Eng. J. 389 (2020) 123918, https://doi.org/10.1016/j.cej.2019.123918.

[37] S.S. Sahoo, S. Mansingh, P. Babu, K. Parida, Black titania an emerging photocatalyst: review highlighting the synthesis techniques and photocatalytic activity for hydrogen generation, Nanoscale Adv. 3 (19) (2021) 5487–5524, https://doi.org/10.1039/D1NA00477H.

[38] E.Kusiak Nejman, A. Wanag, J.Kapica Kozar, A. Morawski, Preparation and characterisation of TiO_2 thermally modified with cyclohexane vapours, Int. J. Mater. Prod. Technol. 52 (2016) 286, https://doi.org/10.1504/IJMPT.2016.075501.

[39] L. Hu, Y. Li, W. Zheng, Y.-K. Peng, S.C.E. Tsang, L.Y.S. Lee, K.-Y. Wong, Blue ordered/disordered Janus-type TiO_2 nanoparticles for enhanced photocatalytic hydrogen generation, J. Mater. Chem. A 8 (43) (2020) 22828–22839, https://doi.org/10.1039/D0TA06281B.

[40] S. Rempel, A. Valeeva, E. Bogdanova, N. Sabirzyanov, Development of a biomaterial based on HAP/TiO_y nanocomposite with different stoichiometry, Lett. Mater. 7 (2017) 170–174, https://doi.org/10.22226/2410-3535-2017-2-170-174.

[41] M. Janczarek, M. Endo-Kimura, K. Wang, Z. Wei, M.M.A. Akanda, A. Markowska-Szczupak, B. Ohtani, E. Kowalska, Is black titania a promising photocatalyst? Catalysts 12 (11) (2022) 1320, https://doi.org/10.3390/catal12111320.

[42] D. Ariyanti, L. Mills, J. Dong, Y. Yao, W. Gao, $NaBH_4$ modified TiO_2: defect site enhancement related to its photocatalytic activity, Mater. Chem. Phys. 199 (2017) 571–576, https://doi.org/10.1016/j.matchemphys.2017.07.054.

[43] P. Martelli, R. Caputo, A. Remhof, P. Mauron, A. Borgschulte, A. Züttel, Stability and decomposition of $NaBH_4$, J. Phys. Chem. C 114 (15) (2010) 7173–7177, https://doi.org/10.1021/jp909341z.

[44] H. Tan, Z. Zhao, M. Niu, C. Mao, D. Cao, D. Cheng, P. Feng, Z. Sun, A facile and versatile method for preparation of colored TiO_2 with enhanced solar-driven photocatalytic activity, Nanoscale 6 (17) (2014) 10216–10223, https://doi.org/10.1039/C4NR02677B.

[45] D.-H. Yoon, M.R.U.D. Biswas, A. Sakthisabarimoorthi, Impact of crystalline core/amorphous shell structured black TiO_2 nanoparticles on photoelectrochemical water splitting, Opt. Mater. 133 (2022) 113030, https://doi.org/10.1016/j.optmat.2022.113030.

[46] S. Challagulla, K. Tarafder, R. Ganesan, S. Roy, Structure sensitive photocatalytic reduction of nitroarenes over TiO_2, Sci. Rep. 7 (1) (2017) 8783, https://doi.org/10.1038/s41598-017-08599-2.

[47] O.H.M. El-Banna, W.M. Haggag, N.A. Al-Ansary, Biological products to control grapevine die back pathogen, J. Chem. Pharm. Res. 7 (11) (2015) 545–555.

[48] M. Wajid Shah, Y. Zhu, X. Fan, J. Zhao, Y. Li, S. Asim, C. Wang, Facile synthesis of defective TiO_{2-x} nanocrystals with high surface area and tailoring bandgap for visible-light photocatalysis, Sci. Rep. 5 (1) (2015) 15804, https://doi.org/10.1038/srep15804.

[49] J. Xu, Y. Chen, Z. Dong, Q. Wang, Y. Situ, H. Huang, Facile synthesis of the Ti^{3+}–TiO_2–rGO compound with controllable visible light photocatalytic performance: GO regulating lattice defects, J. Mater. Sci. 53 (18) (2018) 12770–12780, https://doi.org/10.1007/s10853-018-2383-4.

[50] D.C. Hurum, A.G. Agrios, K.A. Gray, T. Rajh, M.C. Thurnauer, Explaining the enhanced photocatalytic activity of degussa P25 mixed-phase TiO_2 using EPR, J. Phys. Chem. B 107 (19) (2003) 4545–4549, https://doi.org/10.1021/jp0273934.

[51] S. Livraghi, M. Chiesa, M.C. Paganini, E. Giamello, On the nature of reduced states in titanium dioxide as monitored by electron paramagnetic resonance. I: the anatase case, J. Phys. Chem. C 115 (51) (2011) 25413–25421, https://doi.org/10.1021/jp209075m.

[52] A. Naldoni, M. Altomare, G. Zoppellaro, N. Liu, Š. Kment, R. Zbořil, P. Schmuki, Photocatalysis with reduced TiO_2: from black TiO_2 to cocatalyst-free hydrogen production, ACS Catal. 9 (1) (2019) 345–364, https://doi.org/10.1021/acscatal.8b04068.

[53] Z. Bad'ura, A. Naldoni, S. Qin, A. Bakandritsos, Š. Kment, P. Schmuki, G. Zoppellaro, Light-induced migration of spin defects in TiO_2 nanosystems and their contribution to the H_2 evolution catalysis from water, ChemSusChem 14 (20) (2021) 4408–4414, https://doi.org/10.1002/cssc.202101218.

[54] I. KRONOS Worldwide, Sustainability Report 2015/2016, 5430 LBJ Freeway, Suite 1700 | Dallas, TX, 75240 USA, 2017.

[55] Zakłady Chemiczne Police S.A., Technology. ⟨https://tytanpol.com/en/technologia/proces-technologiczny/⟩.

[56] D. Dolat, D. Moszyński, N. Guskos, B. Ohtani, A.W. Morawski, Preparation of photoactive nitrogen-doped rutile, Appl. Surf. Sci. 266 (2013) 410–419, https://doi.org/10.1016/j.apsusc.2012.12.048.

[57] K. Bubacz, J. Choina, D. Dolat, E. Borowiak-Paleń, D. Moszyński, A.W. Morawski, Studies on nitrogen modified TiO_2 photocatalyst prepared in different conditions, Mater. Res. Bull. 45 (9) (2010) 1085–1091, https://doi.org/10.1016/j.materresbull.2010.06.024.

[58] L. Liu, X. Gu, C. Sun, H. Li, Y. Deng, F. Gao, L. Dong, In situ loading of ultra-small Cu_2O particles on TiO_2 nanosheets to enhance the visible-light photoactivity, Nanoscale 4 (20) (2012) 6351–6359, https://doi.org/10.1039/C2NR31859H.

[59] M.E. KİBar, Preparation of black-titanium dioxide nanotubes by thermal decomposition of sodium borohydride, J. Adv. Res. Nat. Appl. Sci. (Online) 7 (1) (2021) 71–81, https://doi.org/10.28979/jarnas.833273.

[60] L. Han, B. Su, G. Liu, Z. Ma, X. An, Synthesis of oxygen vacancy-rich black TiO_2 nanoparticles and the visible light photocatalytic performance, Mol. Catal. 456 (2018) 96–101, https://doi.org/10.1016/j.mcat.2018.07.006.

[61] P. Makuła, M. Pacia, W. Macyk, How to correctly determine the band gap energy of modified semiconductor photocatalysts based on UV–vis spectra, J. Phys. Chem. Lett. 9 (23) (2018) 6814–6817, https://doi.org/10.1021/acs.jpclett.8b02892.

[62] A. Pérez-Larios, M.I. Torres-Ramos, O.A. González-Vargas, J.L. Rico, R. Zanella, Ti–Fe mixed oxides as photocatalysts in the generation of hydrogen under UV-light irradiation, Int. J. Hydrog. Energy 47 (70) (2022) 30178–30186, https://doi.org/10.1016/j.ijhydene.2022.04.179.

[63] C. Dwivedi, T. Mohammad, V. Kumar, V. Dutta, Ti^{3+} and oxygen defects controlled colored TiO_2 nanoparticles by continuous spray pyrolysis, Vacuum 182 (2020) 109612, https://doi.org/10.1016/j.vacuum.2020.109612.

[64] C.-C. Wang, C.-Y. Chou, The effects of sodium content and hydrogenation of TiO_2 nanotubes on photocatalytic activity, J. Photochem. Photobiol. A: Chem. 358 (2018) 226–235, https://doi.org/10.1016/j.jphotochem.2018.03.029.

[65] K. Alkanad, A. Hezam, N. Al-Zaqri, M.A. Bajiri, G. Alnaggar, Q.A. Drmosh, H. A. Almukhlifi, L. Neratur Krishnappagowda, One-step hydrothermal synthesis of anatase TiO_2 nanotubes for efficient photocatalytic CO_2 reduction, ACS Omega 7 (43) (2022) 38686–38699, https://doi.org/10.1021/acsomega.2c04211.

[66] V.A. Lebedev, D.A. Kozlov, I.V. Kolesnik, A.S. Poluboyarinov, A.E. Becerikli, W. Grünert, A.V. Garshev, The amorphous phase in titania and its influence on photocatalytic properties, Appl. Catal. B: Environ. 195 (2016) 39–47, https://doi.org/10.1016/j.apcatb.2016.05.010.

[67] H. Xie, N. Li, B. Liu, J. Yang, X. Zhao, Role of sodium ion on TiO_2 photocatalyst: influencing crystallographic properties or serving as the recombination center of charge carriers? J. Phys. Chem. C 120 (19) (2016) 10390–10399, https://doi.org/10.1021/acs.jpcc.6b01730.

[68] X. Liu, H. Xu, L.R. Grabstanowicz, S. Gao, Z. Lou, W. Wang, B. huang, Y. Dai, T. Xu, Ti^{3+} self-doped TiO_{2-x} anatase nanoparticles via oxidation of TiH_2 in H_2O_2, Catal. Today 225 (2014) 80–89, https://doi.org/10.1016/j.cattod.2013.08.025.

[69] Y. Yan, H. Yang, X. Zhao, R. Li, X. Wang, Enhanced photocatalytic activity of surface disorder-engineered $CaTiO_3$, Mater. Res. Bull. 105 (2018) 286–290, https://doi.org/10.1016/j.materresbull.2018.05.008.

[70] S. Sorcar, Y. Hwang, C.A. Grimes, S.-I. In, Highly enhanced and stable activity of defect-induced titania nanoparticles for solar light-driven CO_2 reduction into CH_4, Mater. Today 20 (9) (2017) 507–515, https://doi.org/10.1016/j.mattod.2017.09.005.

[71] H. Xu, Z. Wang, H. Liao, D. Li, J. Shen, J. Long, W. Dai, X. Wang, Z. Zhang, Proximity of defects and Ti-H on hydrogenated $SrTiO_3$ mediated photocatalytic reduction of CO_2 to C_2H_2, Appl. Catal. B: Environ. 336 (2023) 122935, https://doi.org/10.1016/j.apcatb.2023.122935.